ADVANCED FUNCTIONAL MATERIALS
www.afm-journal.de

Molecular Heterojunctions of Oligo(phenylene ethynylene)s with Linear to Cruciform Framework

Zhongming Wei, Tim Hansen, Marco Santella, Xintai Wang, Christian R. Parker, Xingbin Jiang, Tao Li, Magni Glyvradal, Karsten Jennum, Emil Glibstrup, Nicolas Bovet, Xiaowei Wang, Wenping Hu, Gemma C. Solomon, Mogens Brøndsted Nielsen, Xiaohui Qiu, Thomas Bjørnholm, Kasper Nørgaard, and Bo W. Laursen**

Electrical transport properties of molecular junctions are fundamentally affected by the energy alignment between molecular frontier orbitals (highest occupied molecular orbital (HOMO) or lowest unoccupied molecular orbital (LUMO)) and Fermi level (or work function) of electrode metals. Dithiafulvene (DTF) is used as substituent group to the oligo(phenylene ethynylene) (OPE) molecular wires and different molecular structures based on OPE3 backbone (with linear to cruciform framework) are achieved, with viable molecular orbitals and HOMO–LUMO energy gaps. OPE3, OPE3–DTF, and OPE3–tetrathiafulvalene (TTF) can form good self-assembled monolayers (SAMs) on Au substrates. Molecular heterojunctions based on these SAMs are investigated using conducting probe–atomic force microscopy with different tips (Ag, Au, and Pt) and Fermi levels. The calibrated conductance values follow the sequence OPE3–TTF > OPE3–DTF > OPE3 irrespective of the tip metal. Rectification properties (or diode behavior) are observed in case of the Ag tip for which the work function is furthest from the HOMO levels of the OPE3s. Quantum chemical calculations of the transmission qualitatively agree with the experimental data and reproduce the substituent effect of DTF. Zero-bias conductance, and symmetric or asymmetric couplings to the electrodes are investigated. The results indicate that improved fidelity of molecular transport measurements may be achieved by systematic studies of homologues series of molecular wires applying several different metal electrodes.

1. Introduction

After the first theoretical prediction of molecular rectification based on a single organic molecule in 1974,[1] molecular electronics has developed significantly both experimentally and theoretically with the aim to understand and explain structure–property relationships for both molecules and their devices.[2–9] In solid-state devices, the charge transport properties of molecular systems are strongly dependent on the nature of the molecule and the electrodes, as well as the connection between them. In particular, the strength (weak, intermediate, or strong) of the electronic coupling between molecules and the electrodes plays an important role in the fabrication, measurement, and understanding of single-molecule devices.[2]

It has been reported that the electrical transport and thermoelectric properties of molecular junctions is fundamentally affected by the energy alignment between a molecular frontier orbital (the highest occupied molecular orbital, HOMO, or the lowest unoccupied molecular orbital, LUMO) and the Fermi level (or work function) of electrode metals.[10–13] Consequently, the device performance of molecular junctions can be modulated by tuning the position of the molecular orbitals and/or the Fermi level of the metal electrodes. The molecular orbital landscape is a function of the molecular structure, including the presence of any chemical substituents.[14–16] Changing the conjugation pathway of molecular wires or adding efficient electron donating/withdrawing substituents onto the backbone will shift the relevant

Dr. Z. Wei, T. Hansen, Dr. M. Santella, X. Wang, Dr. C. R. Parker, Dr. T. Li, M. Glyvradal, Dr. K. Jennum, E. Glibstrup, Dr. N. Bovet, Prof. G. C. Solomon, Prof. M. B. Nielsen, Prof. T. Bjørnholm, Prof. K. Nørgaard, Prof. B. W. Laursen
Nano-Science Center and Department of Chemistry
University of Copenhagen
Universitetsparken 5, DK-2100 Copenhagen Ø, Denmark
E-mail: kn@nano.ku.dk; bwl@nano.ku.dk
Dr. Z. Wei
Institute of Semiconductors
Chinese Academy of Sciences
Beijing 100083, P.R. China
X. Jiang, X. Wang, Prof. X. Qiu
National Center for Nanoscience and Technology
Beijing 100190, P.R. China
Prof. W. Hu
Beijing National Laboratory for Molecular Sciences
Key Laboratory of Organic Solids
Institute of Chemistry, Chinese Academy of Sciences
Beijing 100190, P.R. China

DOI: 10.1002/adfm.201404388

orbital energies and has been demonstrated to affect the transport properties of molecular junctions.[17] Electrodes with different work functions can be achieved simply by changing the metal.[18–22] The tips used in conducting probe–atomic force microscopy (CP–AFM) and scanning tunneling microscopy (STM) can be coated with different metals and then utilized as top electrode in molecular junctions with self-assembled monolayers (SAMs) on metal surfaces, thus leading to symmetric or asymmetric device configurations with respect to the work function of the electrodes. Different from the STM method which contact a single or a few molecule(s) in the junction, the CP–AFM technique measure a group of molecules in the SAM. The efficient contact area and thus exact number of contacted molecules are very important to the quantitative interpretation of CP–AFM results.[23] Considering this CP–AFM specific issue, calibration of raw conduction data by contact area (number of molecules in the molecular junctions) can make the conductance data much more useful and reliable.

Besides the fabrication technique for devices, interesting systems are needed for the significant investigation of molecule electronics. With the objective to combine the properties of rigid, highly conjugated oligo(phenylene ethynylene) (OPE) molecular wires, with an extended tetrathiafulvalene (TTF) donor moiety, synthetic protocols for OPE–TTF cruciform molecules in which a π-extended TTF is placed orthogonally to an OPE wire were recently developed.[24–26] In a previous work, we investigated the SAMs of OPE5–TTF and OPE3–TTF in molecular junctions by CP–AFM.[27] The study showed that the TTF substituent increases the conductance of the OPE wire by approximately one order of magnitude, compared to the unsubstituted analogue. This increased molecular conductance was assigned to changes in the molecular orbital energy levels relative to the Fermi level of the applied gold electrodes and a smaller HOMO–LUMO energy gap. Such extended TTF cruciform molecules were also developed with dithiafulvene-4,5-dithiolate anchoring groups and studied in molecular break junctions.[28] A comprehensive study of the extended TTF cruciform molecules for molecular electronics with both the synthetic strategies and electrical transport measurements has recently been reported.[29]

In order to further investigate the origin of the high molecular conduction of these donor substituted OPEs, we here investigated the OPE3 series by also including the redox-active dithiafulvene (DTF) substituents. The structures of three OPE3s with linear to cruciform architecture are shown in **Scheme 1**. The DTF units here contain peripheral *n*-propyl ester groups (CO_2Pr). These groups are convenient from a synthetic point of view and they provide good solubility. Owing to their electron-withdrawing nature, they somewhat reduce the donor strength of the DTF units, which on the other hand increase the chemical stability of the molecules. Molecular junctions of this OPE3 series were obtained by contacting SAMs grown on flat Au surfaces using CP–AFM with different metal tips (Ag, Au, and Pt) to form both symmetric and asymmetric junctions. The observed difference in electrical performance of these molecular junctions as a function of molecular structure and electrode metal is discussed in relation to the difference in alignment of molecular orbitals and Fermi level of the electrodes. The modulation of molecular orbitals and the transmission functions by the different number of DTF substituents were also investigated by theoretical calculation.

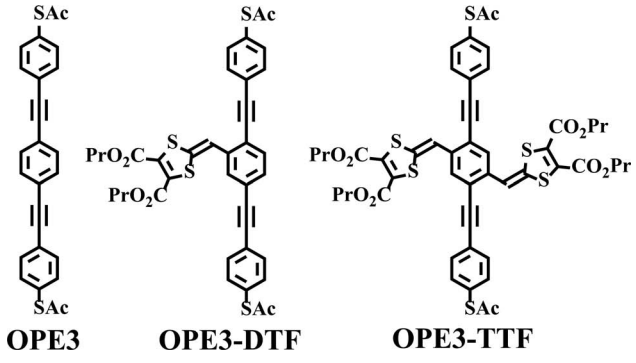

Scheme 1. Molecular structures of OPE3, OPE3–DTF, and OPE3–TTF.

2. Fabrication of SAMs

All three OPE3 molecules form good SAMs on gold following the method of Chiechi.[30,31] The density, stability, and composition of the SAMs were characterized by cyclic voltammetry (CV) and X-ray photoelectron spectroscopy (XPS). For OPE3 and OPE3–TTF, parts of these data were reported previously.[27] In order to investigate the substituent effect of the DTF group on OPE wires, all data for the OPE3 series are summarized in **Table 1**.

The dense coverage of the SAMs on the Au surface was confirmed by cyclic voltammograms showing the attenuation of the signal from Fe^{2+}/Fe^{3+} in water. For SAMs of OPE3 and OPE3–TTF on Au these data are shown in ref. [27] and that of OPE3–DTF is given in Figure S1, Supporting Information. Compared to the bare Au electrode, the peaks for Fe^{2+}/Fe^{3+} redox signal were clearly suppressed after the OPE SAMs covered on Au surface. This observation implies that all three OPE SAMs are densely packed on the Au surface. In order to check the bonding strength between the thiol anchoring group and the Au substrate, we investigated the stability of the OPE3 SAMs by electrochemical reductive desorption as shown in **Figure 1**. For the OPE3 SAM, the desorption peak $E_{desorption}$ (E_D) is around −0.93 V, which is similar to that of octanethiol SAMs[32] (≈ −1.0 V) and implies that the thiol anchoring group binds strongly to the Au substrate. The E_D of OPE3–DTF and OPE3–TTF moves toward less negative potential compare to OPE3, which indicating a slightly lower stability of the SAMs. The full width half maximum (FWHM) of the reductive desorption reflects the uniformity of monolayer. For the nonsubstituted OPE3, a sharp desorption peak with a FWHM of about 66 mV points to a high homogeneity and double electron desorption process, and indicated strong interaction between the thiol anchoring group and Au substrate.[32] For OPE3–DTF and OPE3–TTF, the FWHM value was found to be 191 and 186 mV, respectively. Shoulders can be seen from the voltammograms of the two substituted OPE3s, indicating less uniformity of these SAMs, as different domains of molecules leaves the Au surface at different applied potential. These electrochemical phenomenon of OPE3–DTF and OPE3–TTF SAMs might resulted from two factors: the larger intermolecular distance compare with pure OPE3 backbone,[27] and intrinsic redox active[33] properties of the conjugated DTF substituents.

Table 1. Summary of the SAM properties analyzed from CV and XPS data.

SAM	$E_{desorption}$ [V]	Surface coverage [E-10 mol cm^{-2}]	Single molecular area [Å^2]	Thickness [nm]		Mass area density [E-7 g cm^{-2}]
				DFT length	XPS	
OPE3	−0.93	4.15	40	2.01[a)]	1.8[a)]	1.77
OPE3–DTF	−0.75	2.97	55	2.01	2.0	2.10
OPE3–TTF	−0.49	2.13	78	2.01[a)]	2.4[a)]	2.13

[a)]Data from previously study.[27]

The above results revealed that adding the DTF substituent slightly decreased the stability and uniformity of SAMs, likely due to the relatively larger molecular footprint and lower density of OPE3–DTF and OPE3–TTF SAMs. Table 1 summarizes the single molecular area and surface coverage of the SAMs derived from the electrochemical desorption measurements. The DTF substituents attached to the side of the OPE3 backbone increased the single molecular area by ≈15–18 Å^2 for each DTF group.

In agreement with other reported OPE SAMs,[30,34] XPS analysis in our previous work[27] showed that most of the OPE3 and OPE3–TTF molecules in the SAMs were aligned with the backbone standing vertically on the Au surface. Herein, we examine the XPS of OPE3–DTF SAMs (as shown in Figure S2, Supporting Information). From the S2p signals for the OPE3–DTF SAM, only two types of S atoms were identified: (i) S bound to Au (S–Au, S $2p_{3/2}$ = 162 eV), (ii) S bound to R (S–R, S $2p_{3/2}$ = 164 eV). No oxidation of the S was noticed (S=O, S $2p_{3/2}$ = 168 eV) indicating a homogeneous binding mode and high chemical stability of the SAM. From the integrated signals, the relative intensity of the peaks for S–Au and S–R showed a ratio about 1:2.6, which indicates that nearly all the OPE3–DTF molecules in the SAM are standing up on the Au surface. The thickness of the OPE3 SAMs were estimated from the XPS spectra (by the attenuation of the Au signal[27,30,35]) and are summarized in **Table 2**. Although these three OPE3 molecules have the same simulated length of 2.01 nm, the calculated SAM thickness (from XPS) increased with the number of DTF substituents. That might be a result of increased attenuation (caused by the increasing mass area density as shown in Table 1) of the Au signal as it was buried under a larger number of atoms from the side chains of DTF and TTF. Despite a less coherent packing, the overall density and/or height of the DTF and TTF substituted OPE3 SAMs are slightly larger than that of the OPE3. Yet these variations are small, and no matter if the SAM thickness is estimated by XPS or assumed to be equal to the calculated molecular length similar mass densities of the SAMs are obtained. From the SAM thickness and the mass area density given in Table 1 it can be deduced that the mass density of all three SAMs falls in the range between 0.9 and 1.1 g cm^{-3} which correspond very well to the expected mass density of organic materials, again highlighting that the SAMs display a high coverage.

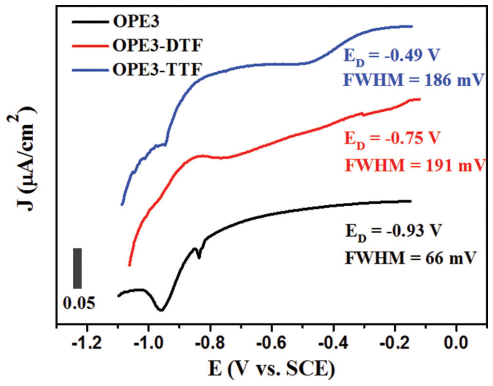

Figure 1. Electrochemical reductive desorption curves for OPE3, OPE3–DTF, and OPE3–TTF SAMs.

3. Fabrication and Measurement of Molecular Heterojunctions

The transport properties of each of the three SAMs were measured by CP–AFM. Ag, Au, and Pt coated conductive tips were used as top electrodes separately, thus vertical device structures were formed, either with symmetric Au/molecular wires/Au junctions or with asymmetric Ag or Pt/molecular wires/Au junctions. We expect that the contact areas in the molecular junctions were almost the same between measurements of different SAMs, as the same tip and soft contact load force value were used for all junctions. However, between different tips these areas should be different due to the different radius caused by thermal deposition of Au and Ag on top of the commercial Pt tips.

Figure 2 shows the average current–voltage (*I–V*) curves of about 200 molecular junction measurements of the three SAMs measured in the three junctions (different metal tips). The *I–V* curves of OPE3–DTF and OPE3–TTF were quite similar and overlap to each other in all three types of junctions. Also, both of them showed higher current than that of OPE3. These results imply that the DTF, which is a strong electron donating group, can efficiently enhance the charge transport through the OPE wire, similar to what has been reported for the TTF system.[27,28]

The average conductance values of the SAM junctions are listed in Table 2. The conductance values (histograms shown in **Figure 3**) were determined over a small bias range of ±0.1 V. From the conductance distribution in Figure 3, we can find that OPE3 always showed sharp peaks at a small value. This indicated the excellent repeatable transport properties for the OPE3 backbone. After adding the DTF or TTF side chains, a large percentage of the conductance appeared with higher values, a

Table 2. Summary of the electrical transport properties of the OPE heterojunctions.

AFM tip [work function, eV]	Average work function [eV]	SAM junction	Junction conductance [nS]	Relative single molecular conductance (G)[a)]	Rectification coefficient
Ag (4.5)	4.8	OPE3	2.23	$G_{OPE3-Ag}$	2.62
		OPE3–DTF	8.14	$5.0 \times G_{OPE3-Ag}$	2.46
		OPE3–TTF	9.76	$8.5 \times G_{OPE3-Ag}$	1.82
Au (5.1)[b)]	5.1	OPE3	1.49	$G_{OPE3-Au}$	1.57
		OPE3–DTF	2.85	$2.6 \times G_{OPE3-Au}$	1.15
		OPE3–TTF	5.56	$7.3 \times G_{OPE3-Au}$	1.03
Pt (5.6)	5.35	OPE3	1.76	$G_{OPE3-Pt}$	1.39
		OPE3–DTF	6.95	$5.4 \times G_{OPE3-Pt}$	1.07
		OPE3–TTF	5.81	$6.4 \times G_{OPE3-Pt}$	1.1

[a)]The relative single molecular conductance was calculated as G = [(junction conductance × single molecular area)/(OPE3 junction conductance × 40 Å^2)]G_{OPE3}; [b)]Also reported in ref. [29].

broader variation in the histograms and larger error bars for the average value were observed. This result also agrees with our above discussion which shows that the addition of a DTF substituent can slightly decrease the uniformity of SAMs. With the relatively larger molecular footprint and lower density for OPE3–DTF and OPE3–TTF SAMs, larger distributions were observed in their molecular junctions.

Due to the size difference between tips of different metals, we only compared these values within the unique group with the same tip (Ag, Au, or Pt). In the heterojunctions with Ag/Au and Au/Au electrodes, the conductance values followed the sequence OPE3–TTF > OPE3–DTF > OPE3. In case of Pt/Au heteroelectrodes, OPE3–DTF showed slightly higher conductance than OPE3–TTF. These values cannot exactly reveal the molecular conductance directly, as there are several tens of molecules trapped in each junction. With the same contact area for a specific tip, the relative number of molecules in the heterojunctions can be calculated for all three OPE wires based on their different single molecular areas estimated for the SAMs (Table 1).

After calibration by the single molecular area, precise information about the relative single molecular transport properties of the OPE wires are obtained (Table 2). For each junction type we calculate this relative single molecular conductance normalized to the conduction of the unsubstituted OPE3 molecular wire (G_{OPE3}), allowing a comparison of the molecular conductance of the OPE wires as a function of substituents. After this calibration with the single molecular areas, the conductance values followed the sequence OPE3–TTF > OPE3–DTF > OPE3 in all three groups of heterojunctions as illustrated in **Figure 4** showing the relative single molecular conductance dependence of average work function of electrodes in the molecular heterojunctions.

Regardless of the work function of the top electrode (tip), the same trend of conductance for the OPEs in different heterojunctions implied a molecular origin to the observed differences (and a similar mode of conduction) and thus confirmed that molecular junctions are efficiently formed. The electron donating DTF and TTF groups demonstrate a molecular structure–property relationship and functions as efficient tools to modulate the molecular transport characteristics. For single molecular solid state devices, several parameters determine the transport properties. Such parameters include molecular backbone length and conjugation, electronic coupling between molecules and electrodes, contact resistance, conformation of anchoring, and the energy gap between the HOMO and LUMO.[2,27] With the same device structure and molecular length, a significant difference in the OPE heterojunctions, caused by the one or two side substitution of DTF, is the HOMO and LUMO level. Thus, the three OPEs showed different HOMO–LUMO gaps and different alignment of the orbital energies with the electrode Fermi level. The structure of the isolated OPE molecules were optimized using density functional theory (DFT) as shown in Figure S4, Supporting Information.[36] From the calculated molecular orbital energies, we can see that DTF substituents increase both the HOMO and LUMO energy, but the change for HOMO level are more significant (Table S1, Supporting Information). Thus, the HOMO–LUMO gap of the three OPEs appeared to be OPE3–TTF < OPE3–DTF < OPE3. The optical energy gaps (E_g) calculated from the edge of UV–vis absorption of OPEs also showed similar values and a same trend (Table S1, Supporting Information). With the HOMO levels more nearby to the work function of Au electrode, we suggest that the observed increase of single molecular conductance is related to the higher HOMO levels and decrease of HOMO–LUMO gap induced by the DTF and TTF groups. Recently, by using the scanning tunneling microscopy break junction (STM BJ) technique, González *et al.* reported absence of significant changes in the electronic structure and conductance of the diamine anchored OPE3 wires with electron-donating (alkoxy) or withdrawing (–F) substituents.[37] But in contrast, the DTF and TTF groups here remarkably changed the conjugation of OPE backbone and induced much larger difference of molecular orbitals (HOMO).

Rectification (or diode behavior) is an important property of molecular electronics and this phenomenon of asymmetric transport has been reported for many Donor-σ-Acceptor systems[38,39] as well as for fully π-conjugated molecules.[40–42] Rectification in molecular junctions is usually described as a result of intramolecular electron transfer or molecule–metal contact.[43] In our case, where junctions contain a flat gold film as one electrode and a metal AFM tip as the other, the

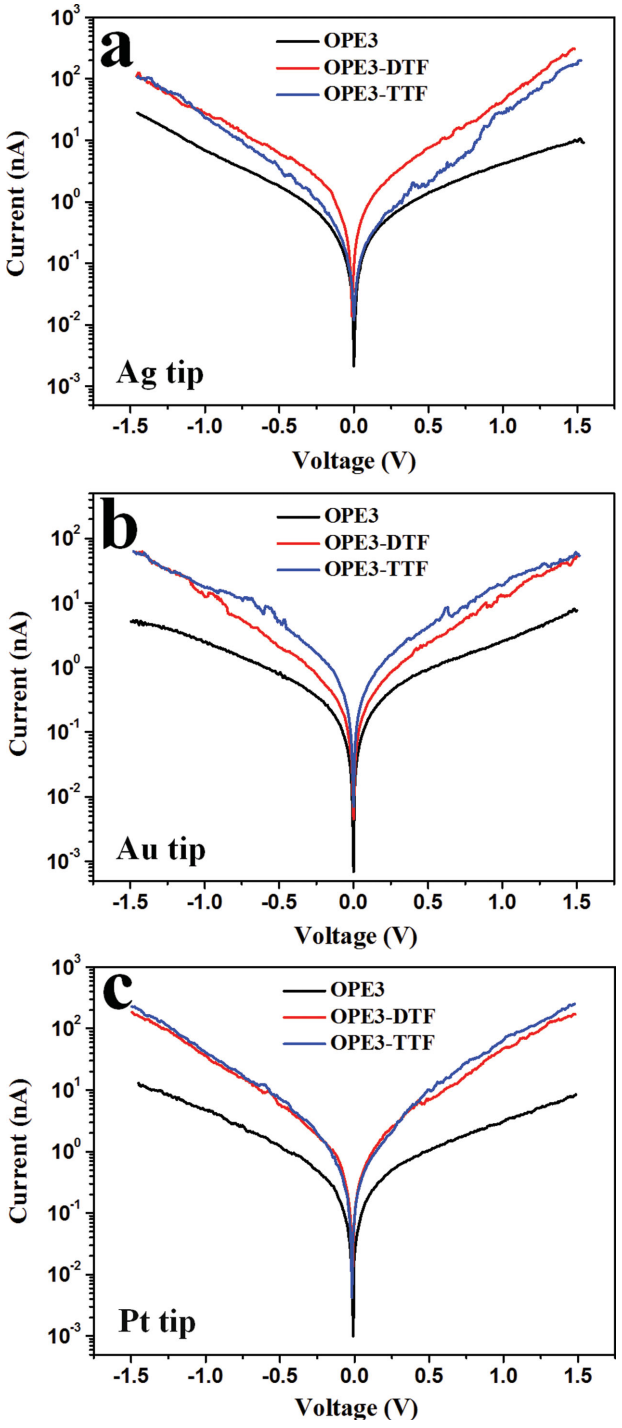

Figure 2. Average *I–V* curves of about 200 molecular junctions based on the OPE SAMs measured by CP–AFM with a) Ag, b) Au, and c) Pt tips.

devices are intrinsically asymmetric, and some degree of rectification can be expected. The calculated rectification coefficient $R(V) = |I(V)|/|I(-V)|$ at a bias voltage of 1.5 V is showed in Table 2. In case of Au and Pt tips, the rectifying effects were small. When using the Ag tip with a lower average work function, clear rectification was observed. This could be induced by the asymmetric alignment between the low work function Ag tip (4.5 eV), and OPE3s HOMO orbitals (shown in Table S1, Supporting Information, all the values were lower than –5.0 eV), and Au substrate under forward and reverse bias. While using the Au and Pt tips, the difference between the electrode's Fermi level and molecular HOMO orbital is smaller resulting in modest rectification coefficients.

4. Theoretical Simulation

In order to compare with "perfect junctions" where the molecules are standing at right angles to planar gold electrodes and the molecular distribution on the electrodes is perfectly isotropic, theoretical modeling of the single molecules in metal junctions was performed, based on the same DFT techniques as the geometry optimizations.[36] Furthermore, to remove any effects the structure of the probe electrode might have, this electrode was also modeled by a flat infinite gold (111) surface.

Figure 5 presents a plot of the logarithm of the transmission as a function of energy relative to the Au Fermi energy (here set to –5.1 eV)[44,45] and the resulting *I–V* curves obtained from integration. From the plot of transmission as shown in Figure 6a, it is possible to estimate where the energy levels of the molecule that dominate the transport (peaks in the transmission function) are located and the size of their couplings to the electrodes (Γ) (given by the broadening of these peaks).

It can be seen that the tail coming down from the HOMO peak dominates the transmission around the Fermi energy and thus the properties of the individual HOMO orbitals will determine the trends in conductance for the molecules. In order to understand these trends, we can consider two parameters of interest. The first is the HOMO orbital energy relative to the Fermi energy, where lower the difference, the higher the conductance at the Fermi energy. The other property is Γ, where the stronger the coupling, the broader the peak, which in turn increases the transmission away from resonance. It can be seen that the absolute difference between the energies of the HOMO orbitals and the Fermi level are ordered as OPE3–TTF < OPE3–DTF < OPE3 with the level close to the Fermi energy, and the couplings are ordered in the same order, giving opposite effects on the zero-bias conductance. From Figure 5a it can be seen that the orbital energy ordering is the determinative factor for these systems.

To have a comparison with experimental results from the heterojunctions, *I–V* curves were constructed from the transmission functions using the following Equation (1):

$$I(V) = \frac{2e}{h}\int_{-\infty}^{\infty} T(E)\left(f\left(E-\frac{eV}{2}\right)-f\left(E+\frac{eV}{2}\right)\right)\mathrm{d}E \quad (1)$$

where $T(E)$ is the transmission function and $f(E)$ is the Fermi function. This equation fails to capture the effect an applied bias has on the molecule and the surrounding environment, but it provides a fast way to calculate an approximate *I–V* curve. The *I–V* curves thus produced are displayed in Figure 5b.

As seen in Figure 5a, the transmission for OPE3–DTF does not go to 1 at the HOMO resonance (–0.46 eV). This indicates asymmetric couplings to the two electrodes, as symmetric couplings will always produce a transmission of exactly 1 at

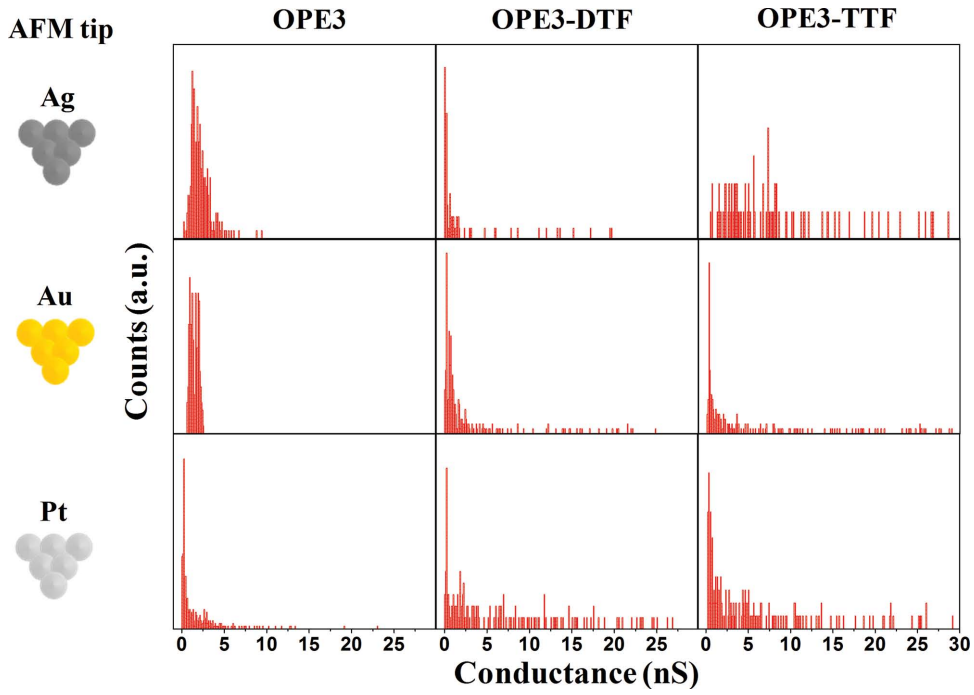

Figure 3. Conductance histograms of the CP–AFM measured OPE molecular heterojunctions.

resonance. The asymmetry in the couplings can be understood by examining the HOMO orbitals on the terminal sulfurs, which are shown in **Figure 6**. Here it can be seen that the electron distributions on the terminal sulfurs have an equal weight, except for those of OPE3–DTF, where a higher density on single terminal sulfur is observed. The electron distributions on the terminal sulfurs can be used as a measure of the couplings for the orbitals with the electrodes, as it is these sulfurs that are responsible for the binding of the molecule to the electrodes. From this it can be expected that the bare molecule OPE3 will have the highest Γ, then OPE3–DTF and OPE3–TTF both being roughly equally small, which is in agreement with what we gathered from the broadening of the peaks in Figure 5a.

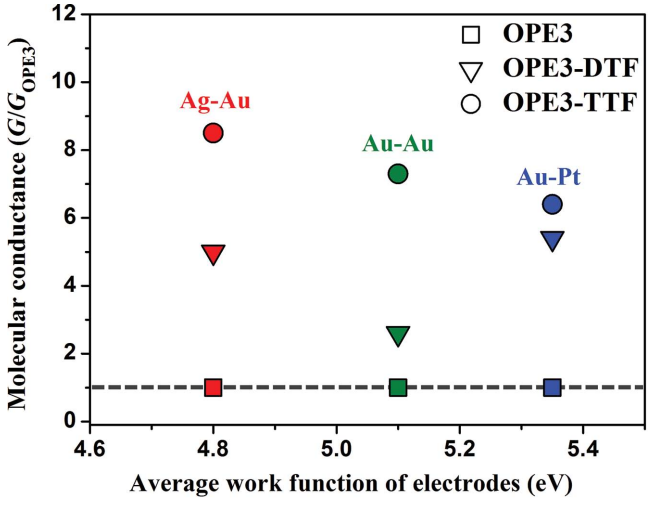

Figure 4. Relative single molecular conductance versus average work function of electrodes in the molecular heterojunctions.

5. Conclusion

In conclusion, the addition of electron donating redox-active dithiafulvene (DTF) as substituent group to the linear OPE3 backbone has yielded different molecular structures (linear to cruciform framework) with different molecular orbitals. SAMs of OPE3, OPE3–DTF, and OPE3–TTF grown on Au substrates were analyzed by CV and XPS. Molecular heterojunctions based on such SAMs were fabricated and measured by CP–AFM. The energy alignment between molecular frontier orbitals and Fermi lever of electrode metals were adjusted both by the different tip coating (Ag, Au, and Pt), and by different HOMO levels induced by DTF group. In all cases, the relative single molecule conductance values followed the sequence OPE3–TTF > OPE3–DTF > OPE3 after calibration. The finding of such uniform transport trends independent of the tip metal coating strongly supports that these observations originates from the intrinsic electronic properties of OPE3 series. The calibration of conductance through the single molecular area also shows to be a valid method to improve the precision of experimental results measured by the CP–AFM technique, which is commonly used in molecular electronics and usually track a group of molecules in the junctions. Rectifiers were obtained when using the Ag tip whose work function is furthest from the transport dominate HOMO levels of the OPEs. Quantum chemical calculations qualitative agree with the experimental data and reproduce the substituent effect of DTF and TTF. Our calculations suggest that the transmissions followed the trend OPE3–TTF > OPE3–DTF > OPE3. We have also seen that data

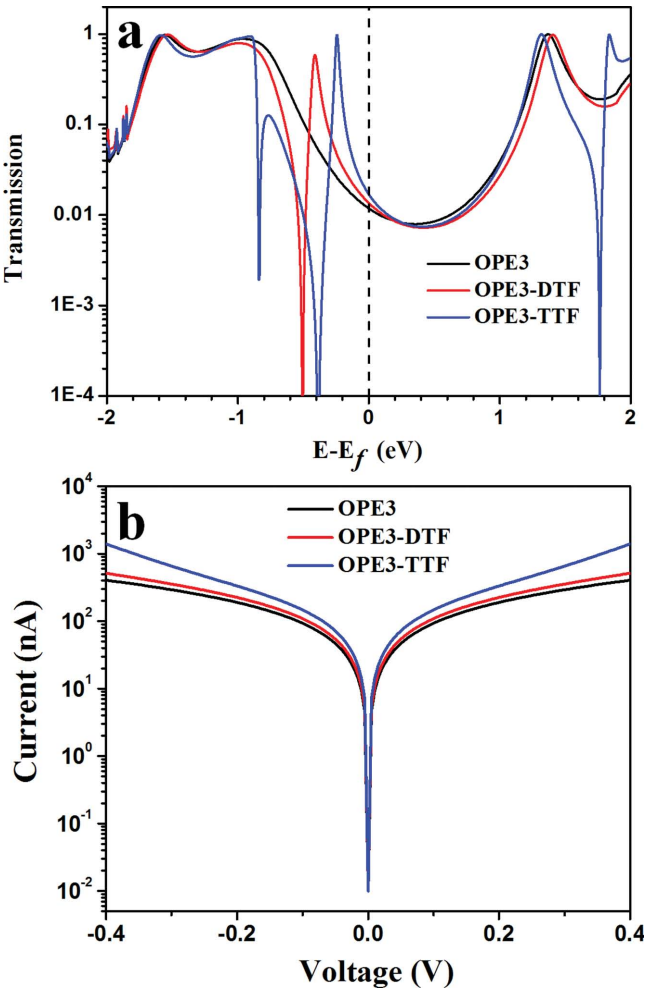

Figure 5. The calculated a) transmission and b) current through the three OPEs (the temperature is set to be 300 K).

for OPE3–DTF should be fitted to an asymmetric coupling matrix, with different couplings to the two electrodes. This may be assigned to the asymmetry of the HOMO orbital of OPE3–DTF. Our results provide additional insights to the structure–property relationships of molecular conductance, as well as new methodologies for improving the reliability of CP–AFM measurements on molecules junctions.

6. Experimental Section

Formation of SAMs: OPE molecules (OPE3–DTF and OPE3–TTF were synthesized as previous reported;[24,27–29] OPE3 was purchased from Sigma-Aldrich) were dissolved at 0.25×10^{-3} M in 15% triethylamine (Et_3N) in tetrahydrofuran (THF) (as reported by Chiechi et al.[30,31]) which had been purged of O_2 with a steady flow of Ar. Freshly stripped ultraflat gold substrates[27] were immediately immersed into the solutions. The containers were filled with Ar and sealed then left with absence of light for 48 h at room temperature to grow the SAMs. After removal from the solutions, the sample was extensively rinsed with THF and ethanol, and then dried under a stream of N_2 before all measurements.

Measurements: CP–AFM measured electrical properties were obtained using a Dimension icon instrument (Veeco) at room temperature in air. For CP–AFM, conductive tip (Veeco model, Scanning capacitancemicroscopy-Pt coated tip (SCM-PIC) Silicon probe, NanoWorld) which had Pt/Cr coated original and followed with 30 nm thermal deposited Au or Ag was used. The *I–V* characteristics of the SAM were measured by a tunneling current AFM application mode of the icon AFM. The conductive tip in contact with SAM was the top electrode and the Au substrate at the bottom of SAM was connected with a conducting wire as one external electrode. The load force was maintained at about 4 nN to achieve a soft contact. *I–V* curves were recorded using a same tip and at different places (at least 100–200 places and two cyclic measurements at each place). Electrochemical measurements were recorded using a three-compartment cell, Electrolytes were prepared from: diluted 70% ultrapure perchloric acid purchased from Sigma Aldrich (concentration = 0.5 M, pH = 1.69), 99% acetic acid/96% sodium acetate buffer (Sigma Aldrich) (pH = 4), and 1 M KCl solution (concentration = 1 M, pH = 6.13). A freshly prepared reversible hydrogen electrode was used as reference electrode and Pt wire was annealed by hydrogen flame and used as counter electrode. The electrolyte solution was degassed with pure Argon for 15 min, about 1 h before measurement. Autolab PGSTAT 12 system controlled by GPES 4.9 software was used for voltammetry test, and reference electrode was calibrated with saturated calomel electrode (SCE) before and after each experiment. Conventional CV were carried in 10×10^{-3} M $K_3Fe(CN)_6/K_4Fe(CN)_6$ solution with 1 M KCl as supporting electrolyte. Electrochemical reductive desorption measurements were in basic solution (KOH, pH > 13), and the corresponding voltage where desorption occurs had been recorded. Purified water (MILLI-Q, 18 MΩ cm) was used throughout, and all glass wares were boiled with 15% nitric acid, wash with MILLI-Q water for several times before use. The single molecular area and surface coverage (Γ) were determined according to Equation (2):[46,47]

$$\Gamma = Q / (nFA) \quad (2)$$

where Q ($Q = It$, I is the current and t is time) is the charge injected into the SAM, n is the number of electrons involved in the electron-transfer process, F is the Faraday constant, and A is the surface area of the monolayer examined in the electrochemical cell. XPS experiments were performed in a Kratos Axis Ultra^{DLD}, fitted with a monochromated Al Kα ($h\nu$ = 1486.6 eV, power = 150 W) X-rays source. The base pressure in the chamber was 5×10^{-10} mbar and never exceeds 5×10^{-9} mbar during an experiment. A pass energy (PE) of 160 eV was used for wide scan and PE = 10 eV for high resolution scan. The data were analyzed with the software casaXPS. All samples were energy calibrated using the Au $4f_{7/2}$ line at 84 eV. The thickness values of OPE3–DTF SAM were obtained follow the same method as previously.[27]

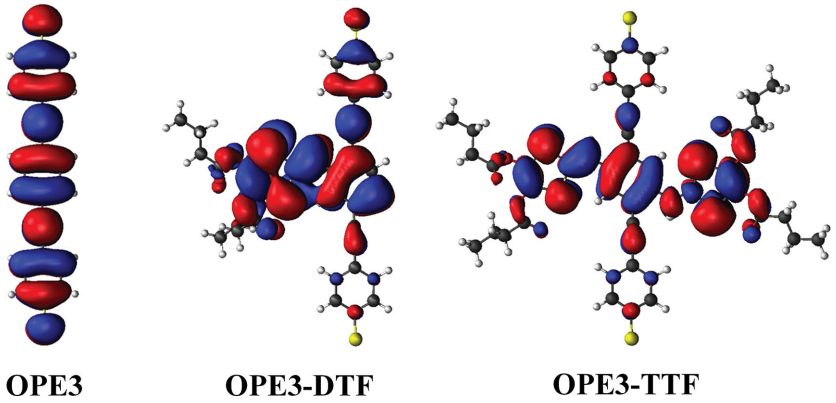

Figure 6. HOMO orbitals of the OPEs.

Quantum Chemical Calculation: The structures of the molecules were optimized in GPAW (a DFT Python code based on the projector-augmented wave (PAW) method)[36,48] using Perdew–Burke–Ernzerhof exchange-correlation functional (PBE)[49] with a double zeta plus polarization (DZp) basis-set.[50] The terminal hydrogen atoms were removed from the optimized structures and then were added two gold (111) slabs with a face-centered cubic (FCC) hollow site chosen as the binding site to the terminal sulfur atoms. The geometries of the molecules appearing in the junctions can be seen in Figure S4, Supporting Information. The Hamiltonians and overlap-matrices of the resulting systems were calculated without further geometry optimization using GPAW with a DZp basis set for the molecule and a single zeta for the gold atoms. The transmission spectra were calculated as literature.[44,45]

Supporting Information

Supporting Information is available from the Wiley Online Library or from the author.

Acknowledgements

The work was supported by the Danish-Chinese Center for Molecular Nanoelectronics funded by the Danish National Research Foundation and the European Union seventh Framework Programme (FP7/2007-2013) under the Grant Agreement No. 270369 (Electric Field Control Over Spin in Molecules, ELFOS).

Received: December 11, 2014
Revised: January 15, 2015
Published online: February 10, 2015

[1] A. Aviram, M. A. Ratner, *Chem. Phys. Lett.* **1974**, *29*, 277.
[2] K. Moth-Poulsen, T. Bjørnholm, *Nat. Nanotechnol.* **2009**, *4*, 551.
[3] T. Li, W. Hu, D. Zhu, *Adv. Mater.* **2010**, *22*, 286.
[4] H. Song, M. A. Reed, T. Lee, *Adv. Mater.* **2011**, *23*, 1583.
[5] T. Li, J. R. Hauptmann, Z. Wei, S. Petersen, N. Bovet, T. Vosch, J. Nygård, W. Hu, Y. Liu, T. Bjørnholm, K. Nørgaard, B. W. Laursen, *Adv. Mater.* **2012**, *24*, 1333.
[6] C. R. Arroyo, S. Tarkuc, R. Frisenda, J. S. Seldenthuis, C. H. M. Woerde, R. Eelkema, F. C. Grozema, H. S. J. van der Zant, *Angew. Chem. Int. Ed.* **2013**, *52*, 3152.
[7] P. Moreno-García, M. Gulcur, D. Z. Manrique, T. Pope, W. Hong, V. Kaliginedi, C. Huang, A. S. Batsanov, M. R. Bryce, C. Lambert, T. Wandlowski, *J. Am. Chem. Soc.* **2013**, *135*, 12228.
[8] E. J. Dell, B. Capozzi, K. H. DuBay, T. C. Berkelbach, J. R. Moreno, D. R. Reichman, L. Venkataraman, L. M. Campos, *J. Am. Chem. Soc.* **2013**, *135*, 11724.
[9] T. Li, M. Jevric, J. R. Hauptmann, R. Hviid, Z. Wei, R. Wang, N. E. A. Reeler, E. Thyrhaug, S. Petersen, J. A. S. Meyer, N. Bovet, T. Vosch, J. Nygård, X. Qiu, W. Hu, Y. Liu, G. C. Solomon, H. G. Kjaergaard, T. Bjørnholm, M. B. Nielsen, B. W. Laursen, K. Nørgaard, *Adv. Mater.* **2013**, *25*, 4164.
[10] L. Venkataraman, Y. S. Park, A. C. Whalley, C. Nuckolls, M. S. Hybertsen, M. L. Steigerwald, *Nano Lett.* **2007**, *7*, 502.
[11] S. K. Yee, J. A. Malen, A. Majumdar, R. A. Segalman, *Nano Lett.* **2011**, *11*, 4089.
[12] J. R. Widawsky, P. Darancet, J. B. Neaton, L. Venkataraman, *Nano Lett.* **2012**, *12*, 354.
[13] H. Nakamura, T. Ohto, T. Ishida, Y. Asai, *J. Am. Chem. Soc.* **2013**, *135*, 16545.
[14] X. Xiao, L. A. Nagahara, A. M. Rawlett, N. Tao, *J. Am. Chem. Soc.* **2005**, *127*, 9235.
[15] L. Venkataraman, J. E. Klare, C. Nuckolls, M. S. Hybertsen, M. L. Steigerwald, *Nature* **2006**, *442*, 904.
[16] J. R. Widawsky, W. Chen, H. Vázquez, T. Kim, R. Breslow, M. S. Hybertsen, L. Venkataraman, *Nano Lett.* **2013**, *13*, 2889.
[17] H. Vazquez, R. Skouta, S. Schneebeli, M. Kamenetska, R. Breslow, L. Venkataraman, M. S. Hybertsen, *Nat. Nanotechnol.* **2012**, *7*, 663.
[18] J. M. Beebe, V. B. Engelkes, L. L. Miller, C. D. Frisbie, *J. Am. Chem. Soc.* **2002**, *124*, 11268.
[19] V. B. Engelkes, J. M. Beebe, C. D. Frisbie, *J. Am. Chem. Soc.* **2004**, *126*, 14287.
[20] B. Kim, S. H. Choi, X. Y. Zhu, C. D. Frisbie, *J. Am. Chem. Soc.* **2011**, *133*, 19864.
[21] A. P. Bonifas, R. L. McCreery, *Nat. Nanotechnol.* **2010**, *5*, 612.
[22] C. M. Kim, J. Bechhoefer, *J. Chem. Phys.* **2013**, *138*, 014707.
[23] L. Welte, A. Calzolari, R. Di Felice, F. Zamora, J. Gomez-Herrero, *Nat. Nanotechnol.* **2010**, *5*, 110.
[24] K. Jennum, M. Vestergaard, A. H. Pedersen, J. Fock, J. Jensen, M. Santella, J. J. Led, K. Kilså, T. Bjørnholm, M. B. Nielsen, *Synthesis* **2011**, 539.
[25] J. K. Sørensen, M. Vestergaard, A. Kadziola, K. Kilså, M. B. Nielsen, *Org. Lett.* **2006**, *8*, 1173.
[26] M. Vestergaard, K. Jennum, J. K. Sørensen, K. Kilså, M. B. Nielsen, *J. Org. Chem.* **2008**, *73*, 3175.
[27] Z. Wei, T. Li, K. Jennum, M. Santella, N. Bovet, W. Hu, M. B. Nielsen, T. Bjørnholm, G. C. Solomon, B. W. Laursen, K. Nørgaard, *Langmuir* **2012**, *28*, 4016.
[28] C. R. Parker, Z. Wei, C. R. Arroyo, K. Jennum, T. Li, M. Santella, N. Bovet, G. Zhao, W. Hu, H. S. J. van der Zant, M. Vanin, G. C. Solomon, B. W. Laursen, K. Nørgaard, M. B. Nielsen, *Adv. Mater.* **2013**, *25*, 405.
[29] C. R. Parker, E. Leary, R. Frisenda, Z. Wei, K. S. Jennum, E. Glibstrup, P. B. Abrahamsen, M. Santella, M. A. Christensen, E. A. Della Pia, T. Li, M. T. Gonzalez, X. Jiang, T. J. Morsing, G. Rubio-Bollinger, B. W. Laursen, K. Nørgaard, H. van der Zant, N. Agrait, M. B. Nielsen, *J. Am. Chem. Soc.* **2014**, *136*, 16497.
[30] H. Valkenier, E. H. Huisman, P. A. van Hal, D. M. de Leeuw, R. C. Chiechi, J. C. Hummelen, *J. Am. Chem. Soc.* **2011**, *133*, 4930.
[31] D. Fracasso, H. Valkenier, J. C. Hummelen, G. C. Solomon, R. C. Chiechi, *J. Am. Chem. Soc.* **2011**, *133*, 9556.
[32] P. Morf, F. Raimondi, H.-G. Nothofer, B. Schnyder, A. Yasuda, J. M. Wessels, T. A. Jung, *Langmuir* **2006**, *22*, 658.
[33] G. Chen, I. Mahmud, L. N. Dawe, L. M. Daniels, Y. Zhao, *J. Org. Chem.* **2011**, *76*, 2701.
[34] K. Liu, G. Li, X. Wang, F. Wang, *J. Phys. Chem. C* **2008**, *112*, 4342.
[35] Q. Lu, K. Liu, H. Zhang, Z. Du, X. Wang, F. Wang, *ACS Nano* **2009**, *3*, 3861.
[36] J. Enkovaara, C. Rostgaard, J. J. Mortensen, J. Chen, M. Dułak, L. Ferrighi, J. Gavnholt, C. Glinsvad, V. Haikola, H. A. Hansen, H. H. Kristoffersen, M. Kuisma, A. H. Larsen, L. Lehtovaara, M. Ljungberg, O. Lopez-Acevedo, P. G. Moses, J. Ojanen, T. Olsen, V. Petzold, N. A. Romero, J. Stausholm-Møller, M. Strange, G. A. Tritsaris, M. Vanin, M. Walter, B. Hammer, H. Häkkinen, G. K. H. Madsen, R. M. Nieminen, J. K. Nørskov, M. Puska, T. T. Rantala, J. Schiøtz, K. S. Thygesen, K. W. Jacobsen, *J. Phys.: Condens. Matter* **2010**, *22*, 253202.
[37] M. T. González, X. Zhao, D. Z. Manrique, D. Miguel, E. Leary, M. Gulcur, A. S. Batsanov, G. Rubio-Bollinger, C. J. Lambert, M. R. Bryce, N. Agraït, *J. Phys. Chem. C* **2014**, *118*, 21655.
[38] R. M. Metzger, *Chem. Rev.* **2003**, *103*, 3803.
[39] R. M. Metzger, *Synth. Met.* **2009**, *159*, 2277.
[40] J. G. Kushmerick, *Mater. Today* **2005**, *8*, 26.
[41] J. G. Kushmerick, C. M. Whitaker, S. K. Pollack, T. L. Schull, R. Shashidhar, *Nanotechnology* **2004**, *15*, S489.

[42] I. Díez-Pérez, J. Hihath, Y. Lee, L. Yu, L. Adamska, M. A. Kozhushner, I. I. Oleynik, N. Tao, *Nat. Chem.* **2009**, *1*, 635.
[43] D. Gao, F. Scholz, H.-G. Nothofer, W. E. Ford, U. Scherf, J. M. Wessels, A. Yasuda, F. von Wrochem, *J. Am. Chem. Soc.* **2011**, *133*, 5921.
[44] M. Strange, I. S. Kristensen, K. S. Thygesen, K. W. Jacobsen, *J. Chem. Phys.* **2008**, *128*, 114714.
[45] J. Chen, K. S. Thygesen, K. W. Jacobsen, *Phys. Rev. B* **2012**, *85*, 155140.
[46] S. H. Choi, C. Risko, M. C. R. Delgado, B. Kim, J.-L. Brédas, C. D. Frisbie, *J. Am. Chem. Soc.* **2010**, *132*, 4358.
[47] S. H. Choi, C. D. Frisbie, *J. Am. Chem. Soc.* **2010**, *132*, 16191.
[48] J. J. Mortensen, L. B. Hansen, K. W. Jacobsen, *Phys. Rev. B* **2005**, *71*, 035109.
[49] J. P. Perdew, K. Burke, Y. Wang, *Phys. Rev. B* **1996**, *54*, 16533.
[50] A. H. Larsen, M. Vanin, J. J. Mortensen, K. S. Thygesen, K. W. Jacobsen, *Phys. Rev. B* **2009**, *80*, 195112.